Synsint Research Group

Available online at www.synsint.com

Synthesis and Sintering

ISSN 2564-0186 (Print), **ISSN** 2564-0194 (Online)

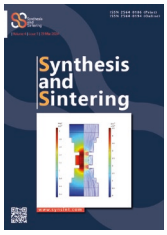

Research article

Solid-solution phase formation rules for high entropy alloys: A thermodynamic perspective

Samaneh Mamnooni [a], **Ehsan Borhani** [a,*], **Hassan Heydari** [b]

[a] *Department of New Science and Technology, Nanomaterials Group, Semnan University, Semnan, Iran*
[b] *Department of Materials and Metallurgical Engineering, Semnan University, Semnan, Iran*

ABSTRACT

To save time and money before starting the production of a high entropy alloy (HEA), it is important to predict the possibility of HEA formation and the probable final microstructure using the solid solution phase formation thermodynamic rules. In this research, a step-by-step calculation of thermodynamic parameters is conducted to predict the possibility of formation and determine the final properties such as ΔH_{mix}, ΔS_{mix}, δr, $\delta\chi$, Ω, VEC, and T_m for three $Ni_{20}Co_{20}Cu_{15}Fe_{20}Mn_{25}$, $Ni_{35}Co_{20}Cu_5Fe_5Mn_{35}$, and $Ni_5Co_5Cu_{35}Fe_{35}Mn_{20}$ HEAs. Based on the obtained results, it is not possible to form a HEA with a solid solution structure for the $Ni_{35}Co_{20}Cu_5Fe_5Mn_{35}$ and $Ni_5Co_5Cu_{35}Fe_{35}Mn_{20}$ systems due to a low ΔS_{mix} value of 11.28 $J.mol^{-1}.K^{-1}$. Based on the calculated values of ΔH_{mix}, intermetallic compound formation and segregation are predicted for $Ni_{35}Co_{20}Cu_5Fe_5Mn_{35}$ and $Ni_5Co_5Cu_{35}Fe_{35}Mn_{20}$, respectively.

KEYWORDS

High entropy alloy
Thermodynamic parameters
Solid solution
Phase formation
Segregation
Intermetallic compound

OPEN ACCESS

1. Introduction

In conventional alloys, one element was known as the dominant element, and other elements were added to less than 5 at%. With the rapid development of technologies and the need to develop advanced materials, the number of constituent principal elements gradually increased from one to two or more. For example, in intermetallic-based alloys, usually, two elements are considered as dominant elements and the remaining elements are added in small amounts. It was believed that alloys containing three or more principal elements would be complex in terms of microstructure and analysis [1]. The advancement of alloys has been defined as microstructure modification [2–4], mechanical properties enhancement [5–7], adding a new alloy element [8, 9], or surface modification [10] on the existing alloys.

The first results regarding high entropy alloys [11–15] or multi-component alloys [16] were reported in 2004, about 20 years ago. With the introduction of high entropy alloys by Yeh et al. [13] and Cantor et al. [16], the old belief about the complexity of the microstructure when using a large number of main elements was broken. Unlike conventional alloys that contain 1 or 2 main elements, high entropy alloys consist of at least 5 principal elements and the amount of each of these elements varies between 5 and 35% [13, 17–24]. By a combination of five or more elements from the periodic table, millions of alloys can be achieved, and an unlimited number of microstructures are obtained for each composition. Each of these microstructures has rare physical and mechanical properties [25].

The name selected for high-entropy alloys is borrowed from their configurational entropy, although magnetic, electronic, and vibrational entropies are also essential in determining phase stability [26]. The elevated mixing entropy attributed to multi-principal element alloys causes sluggish cooperative diffusion and lattice distortion. These alloys have a higher propensity to form solid solutions and amorphous phases rather than intermetallic phases. Also, through an attentive selection of small-size factors, the formation of amorphous phases can be blocked in competition with the solid solution phase (BCC/FCC or both) [27–30].

* Corresponding author. *E-mail address:* E.Borhani@semnan.ac.ir (E. Borhani)
Received 29 November 2023; Received in revised form 24 March 2024; Accepted 25 March 2024.

https://doi.org/10.53063/synsint.2024.41192

Of course, any combination of 5 or more elements does not lead to a high entropy alloy with desirable microstructure and properties [31]. In some compounds, there is a possibility of forming a large number of intermetallic phases, which will ultimately cause the sample to become brittle and cause problems in the production and analysis of the final product [32]. Also, by choosing the right combination, it is possible to predict and achieve a high entropy alloy with a solid solution structure and the desired crystal structure (FCC, BCC, etc.) [33]. Solid solution phase formation rules determine the possibility of forming or not forming a high entropy alloy with desirable properties for a unique composition [31, 33].

The final microstructure and design lead to achieving excellent properties such as high plasticity, good fracture toughness, high strength, excellent oxidation, and corrosion resistance, incredible specific strength at elevated temperatures, superconductivity, ductility at low temperatures, high hardness, superior mechanical performance, and microstructure stability at high temperatures [12, 14, 21, 22, 30, 34–44].

According to the mentioned cases, it seems important to use, determine, and calculate solid solution phase formation rules before starting to produce a high entropy alloy. These rules are carefully explained in various studies. However, the void of doing step-by-step and detailed calculations of each of these rules to understand them accurately is felt by researchers who are planning to start the synthesis of a high entropy alloy for the first time. Therefore, in this article, we have performed step-by-step solid solution formation rules calculations for 3 different components.

2. Solid solution formation rules

Yeh et al. [13] predicted the production of HEAs containing several prominent elements based on the ΔS_{mix} parameter. For a multi-principal high entropy alloy, ΔS_{mix} parameter can be calculated using the following Eq. 1 [13, 45]:

$$\Delta S_{mix} = -R\sum_{i=1}^{n}\left(c_i \mathrm{Ln} c_i\right) \quad (1)$$

where R represents the universal gas constant (8.314 $J.mol^{-1}.K^{-1}$), c_i is the atomic percentage related to the i^{th} component element and n is the number of components. At the beginning of the discovery of HEAs, the $\Delta S_{mix} \geq 13.38$ $J.mol^{-1}.K^{-1}$ conditions were considered sufficient to achieve a HEA and the lack of simultaneous intermetallic or other complex phase production [13, 45, 46]. Based on $\Delta G_{mix} = \Delta H_{mix} - T\Delta S_{mix}$ equation, the higher ΔS_{mix} causes the decrease in the ΔG_{mix} parameter especially at high temperatures, where ΔH_{mix} is the enthalpy of mixing and ΔG_{mix} represents the Gibbs free energy of mixing. Of course, the high value of ΔS_{mix} parameter does not absolutely decrease the value of ΔG_{mix} and this parameter alone (ΔS_{mix}) is incomplete for certifying the production of an HEA solid solution [45, 47, 48].

To ensure production of an HEA, the empirical parameter of atomic size difference ($\delta r \leq 6.6\%$) and scaled ratio of ΔS_{mix} to ΔH_{mix} ($\Omega \geq 1.1$) were used [49]:

$$\Omega = \frac{T_m \Delta S_{mix}}{|\Delta H_{mix}|} \quad (2)$$

$$\delta r = \sqrt{\sum_{i=1}^{n} c_i \left(1 - r_i / \sum_{i=1}^{n} c_i r_i\right)^2} \quad (3)$$

where r_i is the atomic radius of the i^{th} component and $(T_m)_i$ in the $T_m = \sum_{i=1}^{n} c_i (T_m)_i$ represents the melting point of the i^{th} constituent element [49]. ΔH_{mix} and $\delta\chi$ (Pauling electronegativity difference) can be determined through the Eq. 4 and Eq. 5, respectively [49, 50]:

$$\Delta H_{mix} = \sum_{i=1, i\neq j}^{n} 4\Delta H_{ij}^{mix} c_i c_j \quad (4)$$

$$\delta\chi = \sqrt{\sum_{i=1}^{n} c_i \left(\chi_i - \sum_{i=1}^{n} c_i \chi_i\right)^2} \quad (5)$$

where ΔH_{ij}^{mix} represents the enthalpy of mixing of the i^{th} and the j^{th} components, c_j defines the atomic percentage of the j^{th} component element, and χ_i means electronegativity related to the i^{th} constituent element [49, 50].

Also, to predict the crystalline structure related to the resulting solid solution, the valence electron concentration (VEC) parameter is determined according to the following equation, where VEC_i is the VEC related to i^{th} component [51, 52]:

$$VEC = \sum_{i=1}^{n} c_i (VEC)_i \quad (6)$$

3. Thermodynamic parameters calculation

3.1. ΔS_{mix} calculation for HEAs

At the first step of ΔS_{mix} calculation, Ln c_i is determined for each of the elements, and then Ln c_i is multiplied by c_i for all of the elements. In the next step, the sum of the numbers obtained for all elements in the previous step is calculated. Then sum of the obtained values is multiplied by the -R number (-8.314). The result of this calculation is reported as the entropy of mixing (ΔS_{mix} ((J/mol.K)) in Tables 1–3.

Table 1. Simulation results of ΔS_{mix} for $Ni_{20}Co_{20}Cu_{15}Fe_{20}Mn_{25}$ HEA.

Elements	Ni	Co	Cu	Fe	Mn
Atomic concentration	0.2	0.2	0.15	0.2	0.25
Ln(atomic concentration)	-1.6094379	-1.6094379	-1.89712	-1.6094379	-1.3862944
(Ln(atomic concentration))×(atomic concentration)	-0.3218876	-0.3218876	-0.284568	-0.3218876	-0.3465736
Sum of last step	-1.596804335				
Sum×(-8.314)	13.27583125				
Entropy of mixing (ΔS_{mix} (J/mol.K))	13.27583125				

Table 2. Simulation results of ΔS_{mix} for $Ni_{35}Co_{20}Cu_5Fe_5Mn_{35}$ HEA.

Elements	Ni	Co	Cu	Fe	Mn
Atomic concentration	0.35	0.2	0.05	0.05	0.35
Ln(atomic concentration)	-1.0498221	-1.6094379	-2.9957323	-2.9957323	-1.0498221
(Ln(atomic concentration))×(atomic concentration)	-0.3674377	-0.3218876	-0.1497866	-0.1497866	-0.3674377
Sum of last step	-1.356336297				
Sum×(-8.314)	11.27657997				
Entropy of mixing (ΔS_{mix} (J/mol.K))	11.27657997				

Table 3. Simulation results of ΔS_{mix} for $Ni_5Co_5Cu_{35}Fe_{35}Mn_{20}$ HEA.

Elements	Ni	Co	Cu	Fe	Mn
Atomic concentration	0.05	0.05	0.35	0.35	0.2
Ln(atomic concentration)	-2.9957323	-2.9957323	-1.0498221	-1.0498221	-1.6094379
(Ln(atomic concentration))×(atomic concentration)	-0.1497866	-0.1497866	-0.3674377	-0.3674377	-0.3218876
Sum of last step	-1.356336297				
Sum×(-8.314)	11.27657997				
Entropy of mixing (ΔS_{mix} (J/mol.K))	11.27657997				

3.2. T_m calculation for HEAs

For T_m calculation first, the melting point of each element was multiplied by the c_i of that element in the main compound. Then, the sum of the values was calculated. Finally, the resulting number was reported as the melting point (T_m (K)) in Tables 4–6.

3.3. ΔH_{mix} calculation for HEAs

At the first step of ΔH_{mix} calculation, the mixing enthalpy of each atomic-pairs (i and j) were multiplied by c_i and c_j and the number 4. In the next step, the sum of all the calculated values at the last step is determined and is reported as enthalpy of mixing (ΔH_{mix} (kJ/mol)) in Tables 7–9.

Table 4. Simulation results of T_m for $Ni_{20}Co_{20}Cu_{15}Fe_{20}Mn_{25}$ HEA.

Elements	Ni	Co	Cu	Fe	Mn
Atomic concentration	0.2	0.2	0.15	0.2	0.25
Melting point (K)	1728	1768	1358	1811	1519
(Melting point)×(atomic concentration)	345.6	353.6	203.7	362.2	379.75
Sum of last step	1644.85				
Melting point (T_m (K))	1644.85				

Table 5. Simulation results of T_m for $Ni_{35}Co_{20}Cu_5Fe_5Mn_{35}$ HEA.

Elements	Ni	Co	Cu	Fe	Mn
Atomic concentration	0.35	0.2	0.05	0.05	0.35
Melting point (K)	1728	1768	1358	1811	1519
(Melting point)×(atomic concentration)	604.8	353.6	67.9	90.55	531.65
Sum of last step			1648.5		
Melting point (T_m (K))			1648.5		

Table 6. Simulation results of T_m for $Ni_5Co_5Cu_{35}Fe_{35}Mn_{20}$ HEA.

Elements	Ni	Co	Cu	Fe	Mn
Atomic concentration	0.05	0.05	0.35	0.35	0.2
Melting point	1728	1768	1358	1811	1519
(Melting point))×(atomic concentration)	86.4	88.4	475.3	633.85	303.8
Sum of last step			1587.75		
Melting point (T_m (K))			1587.75		

Table 7. Simulation results of ΔH_{mix} for $Ni_{20}Co_{20}Cu_{15}Fe_{20}Mn_{25}$ HEA.

Elements	Ni	Co	Cu	Fe	Mn
Atomic concentration	0.2	0.2	0.15	0.2	0.25
ΔH_{mix} (AB)	Ni-Co	Ni-Cu	Ni-Fe	Ni-Mn	Co-Cu
	0	4	-2	-8	6
	Co-Fe	Co-Mn	Cu-Fe	Cu-Mn	Fe-Mn
	-1	-5	13	4	0
4×(atomic concentration (A))×(atomic concentration (B))×(ΔH_{mix} (AB))	Ni-Co	Ni-Cu	Ni-Fe	Ni-Mn	Co-Cu
	0	0.48	-0.32	-1.6	0.72
	Co-Fe	Co-Mn	Cu-Fe	Cu-Mn	Fe-Mn
	-0.16	-1	1.56	0.6	0
Sum of last step			0.28		
Enthalpy of mixing (ΔH_{mix} (kJ/mol))			0.28		

Table 8. Simulation results of ΔH_{mix} for $Ni_{35}Co_{20}Cu_5Fe_5Mn_{35}$ HEA.

Elements	**Ni**	**Co**	**Cu**	**Fe**	**Mn**
Atomic concentration	0.35	0.2	0.05	0.05	0.35
ΔH_{mix} (AB)	Ni-Co	Ni-Cu	Ni-Fe	Ni-Mn	Co-Cu
	0	4	-2	-8	6
	Co-Fe	Co-Mn	Cu-Fe	Cu-Mn	Fe-Mn
	-1	-5	13	4	0
4×(atomic concentration (A))×(atomic concentration (B))×(ΔH_{mix} (AB))	Ni-Co	Ni-Cu	Ni-Fe	Ni-Mn	Co-Cu
	0	0.28	-0.14	-3.92	0.24
	Co-Fe	Co-Mn	Cu-Fe	Cu-Mn	Fe-Mn
	-0.04	-1.4	0.13	0.28	0
Sum of last step			-4.57		
Enthalpy of mixing (ΔH_{mix} (kJ/mol))			-4.57		

Table 9. Simulation results of ΔH_{mix} for $Ni_5Co_5Cu_{35}Fe_{35}Mn_{20}$ HEA.

Elements	**Ni**	**Co**	**Cu**	**Fe**	**Mn**
Atomic concentration	0.05	0.05	0.35	0.35	0.2
ΔH_{mix} (AB)	Ni-Co	Ni-Cu	Ni-Fe	Ni-Mn	Co-Cu
	0	4	-2	-8	6
	Co-Fe	Co-Mn	Cu-Fe	Cu-Mn	Fe-Mn
	-1	-5	13	4	0
4×(atomic concentration (A))×(atomic concentration (B))×(ΔH_{mix} (AB))	Ni-Co	Ni-Cu	Ni-Fe	Ni-Mn	Co-Cu
	0	0.28	-0.14	-0.32	0.42
	Co-Fe	Co-Mn	Cu-Fe	Cu-Mn	Fe-Mn
	-0.07	-0.2	6.37	1.12	0
Sum of last step			7.46		
Enthalpy of mixing (ΔH_{mix} (kJ/mol))			7.46		

3.4. Ω calculation for HEAs

To calculate the Ω parameter, the final calculated ΔS_{mix}, melting point, and ΔH_{mix} (absolute value) were considered. In the first step, calculated values for ΔS_{mix} and T_m are multiplied, and then the obtained value is divided by the absolute value of the calculated ΔH_{mix}. Finally, the resulting number was reported as the omega (Ω) in Tables 10–12.

Table 10. Simulation results of Ω for $Ni_{20}Co_{20}Cu_{15}Fe_{20}Mn_{25}$ HEA.

Elements	**Ni**	**Co**	**Cu**	**Fe**	**Mn**
Atomic concentration	0.2	0.2	0.15	0.2	0.25
Entropy of mixing (ΔS_{mix})			13.27583125		
Melting point (T_m)			1644.85		
Enthalpy of mixing (ΔH_{mix})			0.28		
$\lvert$ Enthalpy of mixing (ΔH_{mix}) $\rvert$			0.28		
Omega (Ω)			77.98839651		

Table 11. Simulation results of Ω for $Ni_{35}Co_{20}Cu_5Fe_5Mn_{35}$ HEA.

Elements	Ni	Co	Cu	Fe	Mn
Atomic concentration	0.35	0.2	0.05	0.05	0.35
Entropy of mixing (ΔS_{mix})	11.27657997				
Melting point (T_m)	1648.5				
Enthalpy of mixing (ΔH_{mix})	-4.57				
$\lvert$ Enthalpy of mixing (ΔH_{mix}) $\rvert$	4.57				
Omega (Ω)	4.067711616				

Table 12. Simulation results of Ω for $Ni_5Co_5Cu_{35}Fe_{35}Mn_{20}$ HEA.

Elements	Ni	Co	Cu	Fe	Mn
Atomic concentration	0.05	0.05	0.35	0.35	0.2
Entropy of mixing (ΔS_{mix})	11.27657997				
Melting point (T_m)	1587.75				
Enthalpy of mixing (ΔH_{mix})	7.46				
$\lvert$ Enthalpy of mixing (ΔH_{mix}) $\rvert$	7.46				
Omega (Ω)	2.400052259				

3.5. δr calculation for HEAs

At the beginning of δr calculation, the atomic radius of each element is multiplied by c_i. In the next step, the sum of the obtained values in the previous step is calculated. Then atomic radius of each element is divided by the sum value of the last step. In the next step, the values obtained for each element in the previous step are subtracted by the number 1. Then the value obtained in the previous step was raised to the power of two. In the next step, c_i for each element is multiplied by the value obtained in the previous step. To get the final sum, the values obtained for different elements in the previous step are added together. To calculate δr, it is taken from the final sum value radical. Finally, the resulting number is reported as a percentage of atomic size difference (δr) in Tables 13–15.

Table 13. Simulation results of δr for $Ni_{20}Co_{20}Cu_{15}Fe_{20}Mn_{25}$ HEA.

Elements	Ni	Co	Cu	Fe	Mn
Atomic concentration	0.2	0.2	0.15	0.2	0.25
Atomic radius	1.246	1.251	1.278	1.241	1.35
(Atomic radius)×(atomic concentration)	0.02492	0.02502	0.01917	0.02482	0.03375
Sum of last step	0.12768				
(Atomic radius)/(sum)	0.97587719	0.97979323	1.0009398	0.97196115	1.05733083
1-(atomic radius/sum)	0.02412281	0.02020677	-0.0009398	0.02803885	-0.0573308
$(1-(\text{atomic radius/sum}))^2$	0.00058191	0.00040831	8.833E-07	0.00078618	0.00328682
(Atomic concentration)×$((1-(\text{atomic radius/sum}))^2)$	0.00011638	8.1663E-05	1.325E-07	0.00015724	0.00082171
Sum of last step	0.001177118				
√(Sum of last step)	0.03430916				
(√(Sum of last step))×100	3.430916014				
Atomic size difference (δr)	3.430916014				

Table 14. Simulation results of δr for $Ni_{35}Co_{20}Cu_5Fe_5Mn_{35}$ HEA.

Elements	Ni	Co	Cu	Fe	Mn
Atomic concentration	0.35	0.2	0.05	0.05	0.35
Atomic radius	1.246	1.251	1.278	1.241	1.35
(Atomic radius)×(atomic concentration)	0.04361	0.02502	0.00639	0.006205	0.04725
Sum of last step			0.128475		
(Atomic radius)/(sum)	0.96983849	0.9737303	0.9947461	0.96594668	1.05078809
1-(atomic radius/sum)	0.03016151	0.0262697	0.0052539	0.03405332	-0.0507881
$(1-(\text{atomic radius/sum}))^2$	0.00090972	0.0006901	2.76E-05	0.00115963	0.00257943
$(\text{Atomic concentration})\times((1-(\text{atomic radius/sum}))^2)$	0.0003184	0.00013802	1.38E-06	5.7981E-05	0.0009028
Sum of last step			0.001418582		
√(Sum of last step)			0.037664074		
(√(Sum of last step))×100			3.766407409		
Atomic size difference (δr)			3.766407409		

Table 15. Simulation results of δr for $Ni_5Co_5Cu_{35}Fe_{35}Mn_{20}$ HEA.

Elements	Ni	Co	Cu	Fe	Mn
Atomic concentration	0.05	0.05	0.35	0.35	0.2
Atomic radius	1.246	1.251	1.278	1.241	1.35
(Atomic radius)×(atomic concentration)	0.00623	0.006255	0.04473	0.043435	0.027
Sum of last step			0.12765		
(Atomic radius)/(sum)	0.97610654	0.9800235	1.0011751	0.97218958	1.05757932
1-(atomic radius/sum)	0.02389346	0.0199765	-0.0011751	0.02781042	-0.0575793
$(1-(\text{atomic radius/sum}))^2$	0.0005709	0.00039906	1.381E-06	0.00077342	0.00331538
$(\text{Atomic concentration})\times((1-(\text{atomic radius/sum}))^2)$	2.8545E-05	1.9953E-05	4.833E-07	0.0002707	0.00066308
Sum of last step			0.000982754		
√(Sum of last step)			0.0313489		
(√(Sum of last step))×100			3.134890046		
Atomic size difference (δr)			3.134890046		

3.6. δχ calculation for HEAs

At the first step of δχ calculation, the electronegativity of each element is multiplied by the atomic fraction (c_i) of that element, and then calculates the sum of the obtained values (first sum). Then, for each element, the calculated sum value at the last step is subtracted from the electronegativity of that element. In the next step, the obtained values for each element are raised to the power of two. Then, the obtained values for each element at the previous step are multiplied by the atomic fraction (c_i) of that element. To calculate the final sum, the values calculated in the last step are added together. Finally, to calculate the value of δχ, it is taken from the final calculated value at the last step radical. Finally, the resulting number is reported as Pauling electronegativity difference (δχ) in Tables 16–18.

Table 16. Simulation results of δχ for $Ni_{20}Co_{20}Cu_{15}Fe_{20}Mn_{25}$ HEA.

Elements	Ni	Co	Cu	Fe	Mn
Atomic concentration	0.2	0.2	0.15	0.2	0.25
Electronegativity	1.91	1.88	1.9	1.83	1.55
(Electronegativity)×(atomic concentration)	0.382	0.376	0.285	0.366	0.3875
Sum of last step			1.7965		
(Electronegativity) - (sum)	0.1135	0.0835	0.1035	0.0335	-0.2465
((Electronegativity) - (sum))^2	0.01288225	0.00697225	0.0107123	0.00112225	0.06076225
(((Electronegativity) - (sum))^2)×(atomic concentration)	0.00257645	0.00139445	0.0016068	0.00022445	0.01519056
Sum of last step			0.02099275		
√(Sum of last step)			0.14488875		
Pauling electronegativity difference (δχ)			0.14488875		

Table 17. Simulation results of δχ for $Ni_{35}Co_{20}Cu_5Fe_5Mn_{35}$ HEA.

Elements	Ni	Co	Cu	Fe	Mn
Atomic concentration	0.35	0.2	0.05	0.05	0.35
Electronegativity	1.91	1.88	1.9	1.83	1.55
(Electronegativity)×(atomic concentration)	0.6685	0.376	0.095	0.0915	0.5425
Sum of last step			1.7735		
(Electronegativity) - (sum)	0.1365	0.1065	0.1265	0.0565	-0.2235
((Electronegativity) - (sum))^2	0.01863225	0.01134225	0.0160023	0.00319225	0.04995225
(((Electronegativity) - (sum))^2)×(atomic concentration)	0.00652129	0.00226845	0.0008001	0.00015961	0.01748329
Sum of last step			0.02723275		
√(Sum of last step)			0.165023483		
Pauling electronegativity difference (δχ)			0.165023483		

Table 18. Simulation results of δχ for $Ni_5Co_5Cu_{35}Fe_{35}Mn_{20}$ HEA.

Elements	Ni	Co	Cu	Fe	Mn
Atomic concentration	0.05	0.05	0.35	0.35	0.2
Electronegativity	1.91	1.88	1.9	1.83	1.55
(Electronegativity)×(atomic concentration)	0.0955	0.094	0.665	0.6405	0.31
Sum of last step			1.805		
(Electronegativity) - (sum)	0.105	0.075	0.095	0.025	-0.255
((Electronegativity) - (sum))^2	0.011025	0.005625	0.009025	0.000625	0.065025
(((Electronegativity) - (sum))^2)×(atomic concentration)	0.00055125	0.00028125	0.0031588	0.00021875	0.013005
Sum of last step			0.017215		
√(Sum of last step)			0.131205945		
Pauling electronegativity difference (δχ)			0.131205945		

3.7. VEC calculation for HEAs

To calculate the VEC parameter, at first VEC value of each of the elements is multiplied the by atomic fraction (ci) of that element. At the next step, the sum of the obtained values at the previous step is calculated and reported as valence electron concentration (VEC) value in Tables 19–21.

For a more detailed review and comparison, the summaries of solid solution formation thermodynamic rules calculated for three $Ni_{20}Co_{20}Cu_{15}Fe_{20}Mn_{25}$, $Ni_{35}Co_{20}Cu_5Fe_5Mn_{35}$, and $Ni_5Co_5Cu_{35}Fe_{35}Mn_{20}$ HEAs are given in Tables 22, 23 and 24 respectively. According to Table 22, the values of ΔH_{mix}, ΔS_{mix}, δr, δχ, Ω, VEC and T_m parameters for $Ni_{20}Co_{20}Cu_{15}Fe_{20}Mn_{25}$ HEA were calculated as 0.28 kJ.mol^{-1}, 13.27 J.mol^{-1}.K^{-1}, 3.43%, 0.14%, 77.98, 8.8 and 1645 K (1372 °C), respectively. The value of the ΔS_{mix} parameter (13.27 J.mol^{-1}.K^{-1}) is very close to the initial condition for the possibility of forming a high entropy alloy ($\Delta S_{mix} \geq$ 13.38 J.mol^{-1}.K^{-1}). As mentioned before, the critical condition for solid solution formation is δr ≤ 6.6% and Ω ≥ 1.1. Multicomponent systems with lower Ω and higher δr than critical conditions form intermetallics compounds and bulk metallic glasses (BMGs) [1]. The value of Ω for intermetallics compounds is higher than that of BMGs [1]. Based on the values of δr and Ω calculated for the $Ni_{20}Co_{20}Cu_{15}Fe_{20}Mn_{25}$ compound, the formation of an HEA solid solution can be predicted through synthesis roots. As positive ΔH_{mix} equals to the segregation of atoms, highly negative ΔH_{mix} equals to the formation of intermetallic compounds [53], and a large value related to δχ predicts the possibility of intermetallic formation [54], therefore the low value of ΔH_{mix} (0.28 kJ.mol^{-1}, near zero) and δχ (0.14%) can indicate solid solution phase formation without any segregation or intermetallic phase. According to the calculated value for the VEC parameter (8.8) solid solution with FCC structure production can be predicted when VEC ≥ 8 [52]. These predictions for $Ni_{25}Co_{20}Cu_{10}Fe_{25}Mn_{20}$ HEA have been checked in practical conditions and their correctness has been confirmed by various analyses [33, 55].

According to Table 23, the values of ΔH_{mix}, ΔS_{mix}, δr, δχ, Ω, VEC and T_m parameters for $Ni_{35}Co_{20}Cu_5Fe_5Mn_{35}$ HEA were calculated as

Table 19. Simulation results of VEC for $Ni_{20}Co_{20}Cu_{15}Fe_{20}Mn_{25}$ HEA.

Elements	Ni	Co	Cu	Fe	Mn
Atomic concentration	0.2	0.2	0.15	0.2	0.25
VEC	10	9	11	8	7
(VEC)×(atomic concentration)	2	1.8	1.65	1.6	1.75
Sum of last step			8.8		
Valence electron concentration (VEC)			8.8		

Table 20. Simulation results of VEC for $Ni_{35}Co_{20}Cu_5Fe_5Mn_{35}$ HEA.

Elements	Ni	Co	Cu	Fe	Mn
Atomic concentration	0.35	0.2	0.05	0.05	0.35
VEC	10	9	11	8	7
(VEC)×(atomic concentration)	3.5	1.8	0.55	0.4	2.45
Sum of last step			8.7		
Valence electron concentration (VEC)			8.7		

Table 21. Simulation results of VEC for $Ni_5Co_5Cu_{35}Fe_{35}Mn_{20}$ HEA.

Elements	Ni	Co	Cu	Fe	Mn
Atomic concentration	0.05	0.05	0.35	0.35	0.2
VEC	10	9	11	8	7
(VEC)×(atomic concentration)	0.5	0.45	3.85	2.8	1.4
Sum of last step			9		
Valence electron concentration(VEC)			9		

-4.57 kJ.mol^{-1}, 11.27 J.mol^{-1}.K^{-1}, 3.77%, 0.17%, 4.06, 8.7 and 1649 K (1376 °C), respectively. Also, based on Table 24, the values of ΔH_{mix}, ΔS_{mix}, δr, δχ, Ω, VEC and T_m parameters for $Ni_5Co_5Cu_{35}Fe_{35}Mn_{20}$ HEA were calculated as 7.46 kJ.mol^{-1}, 11.27 J.mol^{-1}.K^{-1}, 3.13%, 0.13%, 2.40, 9 and 1588 K (1315 °C), respectively. Based on the obtained value for the ΔS_{mix} parameter (11.27 J.mol^{-1}.K^{-1}), the initial condition for the synthesis of the $Ni_{35}Co_{20}Cu_5Fe_5Mn_{35}$ and $Ni_5Co_5Cu_{35}Fe_{35}Mn_{20}$ solid solutions ($\Delta S_{mix} \geq$ 13.38 J.mol^{-1}.K^{-1}) was not satisfied. Therefore, it is not expected to achieve the desired high entropy alloys in these systems. In the literature about the $Cu_{35}Co_{35}Ni_{20}Ti_5Al_5$ system, non-achievement of the high entropy alloy during the milling process is also reported due to the too much lower value of ΔS_{mix} parameter (11.28 J.mol^{-1}.K^{-1}) of critical conditions [31].

As previously mentioned, by reducing the value of the ΔH_{mix} parameter from zero to negative numbers, the formation of an intermetallic phase can be predicted. According to the ΔH_{mix} value (-4.57 kJ.mol^{-1}) obtained for $Ni_{35}Co_{20}Cu_5Fe_5Mn_{35}$, there is a possibility of intermetallic phase formation. On the other hand, despite the possibility of segregation of atoms for systems with a very positive ΔH_{mix} parameter value, the possibility of segregation is predicted for $Ni_5Co_5Cu_{35}Fe_{35}Mn_{20}$ system with the ΔH_{mix} parameter value of 7.46 kJ.mol^{-1}.

Table 22. Summary of thermodynamic calculation results for $Ni_{20}Co_{20}Cu_{15}Fe_{20}Mn_{25}$ HEA.

$Ni_{20}Co_{20}Cu_{15}Fe_{20}Mn_{25}$							
Mixing enthalpy (kJ/mol) of atomic-pairs	**Elements**	**Element 1**	**Element 2**	**Element 3**	**Element 4**	**Element 5**	
Elements		**Ni**	**Co**	**Cu**	**Fe**	**Mn**	
Element 1	**Ni**	Ni	0	4	-2	-8	
Element 2	**Co**		Co	6	-1	-5	
Element 3	**Cu**			Cu	13	4	
Element 4	**Fe**				Fe	0	
Element 5	**Mn**					Mn	
		Element 1	**Element 2**	**Element 3**	**Element 4**	**Element 5**	
		Ni	**Co**	**Cu**	**Fe**	**Mn**	
Atomic size (Å)		1.246	1.251	1.278	1.241	1.35	
Composition fraction		0.2	0.2	0.15	0.2	0.25	1
		0.02492	0.02502	0.01917	0.02482	0.03375	0.12768
		0.0001164	8.166E-05	1.325E-07	0.0001572	0.0008217	0.0011771
Atomic size difference (%)							**3.430916**
Melting point (K)		1728	1768	1358	1811	1519	
		345.6	353.6	203.7	362.2	379.75	1644.85
Melting point (K)							**1644.85**
Electronegativity		1.91	1.88	1.9	1.83	1.55	
		0.382	0.376	0.285	0.366	0.3875	1.7965
		0.0025765	0.0013945	0.0016068	0.0002245	0.0151906	0.0209928
Pauling electronegativity difference							**0.1448888**
VEC		10	9	11	8	7	
		2	1.8	1.65	1.6	1.75	8.8
VEC							**8.8**
Enthalpy of mixing (kJ/mol)							**0.28**
Entropy of mixing (J/mol.K)							**13.275831**
Omega							**77.988397**

Table 23. Summary of thermodynamic calculation results for $Ni_{35}Co_{20}Cu_5Fe_5Mn_{35}$ HEA.

$Ni_{35}Co_{20}Cu_5Fe_5Mn_{35}$						
Mixing enthalpy (kJ/mol) of atomic-pairs	**Elements**	**Element 1**	**Element 2**	**Element 3**	**Element 4**	**Element 5**
Elements		**Ni**	**Co**	**Cu**	**Fe**	**Mn**
Element 1	**Ni**	Ni	0	4	-2	-8
Element 2	**Co**		Co	6	-1	-5
Element 3	**Cu**			Cu	13	4
Element 4	**Fe**				Fe	0
Element 5	**Mn**					Mn

	Element 1	**Element 2**	**Element 3**	**Element 4**	**Element 5**	
	Ni	**Co**	**Cu**	**Fe**	**Mn**	
Atomic size (Å)	1.246	1.251	1.278	1.241	1.35	
Composition fraction	0.35	0.2	0.05	0.05	0.35	1
	0.04361	0.02502	0.00639	0.006205	0.04725	0.128475
	0.0003184	0.000138	1.38E-06	5.798E-05	0.0009028	0.0014186
Atomic size difference (%)						**3.7664074**
Melting point (K)	1728	1768	1358	1811	1519	
	604.8	353.6	67.9	90.55	531.65	1648.5
Melting point (K)						1648.5
Electronegativity	1.91	1.88	1.9	1.83	1.55	
	0.6685	0.376	0.095	0.0915	0.5425	1.7735
	0.0065213	0.0022685	0.0008001	0.0001596	0.0174833	0.0272328
Pauling electronegativity difference						**0.1650235**
VEC	10	9	11	8	7	
	3.5	1.8	0.55	0.4	2.45	8.7
VEC						**8.7**
Enthalpy of mixing (kJ/mol)						**-4.57**
Entropy of mixing (J/mol.K)						**11.27658**
Omega						**4.0677116**

Table 24. Summary of thermodynamic calculation results for $Ni_5Co_5Cu_{35}Fe_{35}Mn_{20}$ HEA.

$Ni_5Co_5Cu_{35}Fe_{35}Mn_{20}$							
Mixing enthalpy (kJ/mol) of atomic-pairs	**Elements**	**Element 1**	**Element 2**	**Element 3**	**Element 4**	**Element 5**	
Elements		**Ni**	**Co**	**Cu**	**Fe**	**Mn**	
Element 1	**Ni**	Ni	0	4	-2	-8	
Element 2	**Co**		Co	6	-1	-5	
Element 3	**Cu**			Cu	13	4	
Element 4	**Fe**				Fe	0	
Element 5	**Mn**					Mn	
		Element 1	**Element 2**	**Element 3**	**Element 4**	**Element 5**	
		Ni	**Co**	**Cu**	**Fe**	**Mn**	
Atomic size (Å)		1.246	1.251	1.278	1.241	1.35	
Composition fraction		0.05	0.05	0.35	0.35	0.2	1
		0.00623	0.006255	0.04473	0.043435	0.027	0.12765
		2.854E-05	1.995E-05	4.833E-07	0.0002707	0.0006631	0.0009828
Atomic size difference (%)							**3.13489**
Melting point (K)		1728	1768	1358	1811	1519	
		86.4	88.4	475.3	633.85	303.8	1587.75
Melting point (K)							**1587.75**
Electronegativity		1.91	1.88	1.9	1.83	1.55	
		0.0955	0.094	0.665	0.6405	0.31	1.805
		0.0005513	0.0002813	0.0031588	0.0002188	0.013005	0.017215
Pauling electronegativity difference							**0.1312059**
VEC		10	9	11	8	7	
		0.5	0.45	3.85	2.8	1.4	9
VEC							**9**
Enthalpy of mixing (kJ/mol)							**7.46**
Entropy of mixing (J/mol.K)							**11.27658**
Omega							**2.4000523**

4. Conclusions

In this research, the precise and step-by-step calculation of thermodynamic parameters predicting the possibility of high entropy alloy formation such as ΔH_{mix}, ΔS_{mix}, δr, $\delta\chi$, Ω, VEC and T_m parameters has been done for three $Ni_{20}Co_{20}Cu_{15}Fe_{20}Mn_{25}$, $Ni_{35}Co_{20}Cu_5Fe_5Mn_{35}$ and $Ni_5Co_5Cu_{35}Fe_{35}Mn_{20}$ HEAs. Also, according to the obtained values for each of the solid solution formation rules, possible properties such as the possibility of intermetallic phase formation, segregation, and determination of the final crystal structure are predicted. It will not be possible to form an entropy alloy alloy with a solid solution structure for two $Ni_{35}Co_{20}Cu_5Fe_5Mn_{35}$ and $Ni_5Co_5Cu_{35}Fe_{35}Mn_{20}$ HEAs because of the very low value obtained for the ΔS_{mix} parameter.

CRediT authorship contribution statement

Samaneh Mamnooni: Writing – original draft, Investigation, Formal Analysis, Data curation, Methodology.
Ehsan Borhani: Writing – review & editing, Supervision.
Hassan Heydari: Writing – review & editing.

Data availability

The data underlying this article will be shared on reasonable request to the corresponding author.

Declaration of competing interest

The authors declare no competing interests.

Funding and acknowledgment

This research received no external funding. The authors have no acknowledgments to declare.

References

[1] Y. Zhang, X. Yang, P. Liaw, Alloy design and properties optimization of high-entropy alloys, JOM. 64 (2012) 830–838. https://doi.org/10.1007/s11837-012-0366-5.
[2] S.-Z. Lu, A. Hellawell, Modification of Al-Si alloys: Microstructure, thermal analysis, and mechanisms, JOM. 47 (1995) 38–40. https://doi.org/10.1007/BF03221405.
[3] A. Shamsipoor, B. Mousavi, M.S. Shakeri, Synthesis and sintering of Fe-32Mn-6Si shape memory alloys prepared by mechanical alloying, Synth. Sinter. 2 (2022) 1–8. https://doi.org/10.53063/synsint.2022.2185.
[4] M.S. Kumar, S.R. Begum, M. Vasumathi, C.C. Nguyen, Q. Van Le, Influence of molybdenum content on the microstructure of spark plasma sintered titanium alloys, Synth. Sinter. 1 (2021) 41–47. https://doi.org/10.53063/synsint.2021.1114.
[5] S.-W. Kim, J.K. Hong, Y.-S. Na, J.-T. Yeom, S.E. Kim, Development of TiAl alloys with excellent mechanical properties and oxidation resistance, Mater. Des. (1980–2015) 54 (2014) 814–819. https://doi.org/10.1016/j.matdes.2013.08.083.
[6] T. Zhang, J. Zhu, T. Yang, J. Luan, H. Kong, et al., A new α+ β Ti-alloy with refined microstructures and enhanced mechanical properties in the as-cast state, Scr. Mater. 207 (2022) 114260. https://doi.org/10.1016/j.scriptamat.2021.114260.
[7] M. Akhlaghi, E. Salahi, S.A. Tayebifard, G. Schmidt, Role of SPS temperature and holding time on the properties of Ti3AlC2-doped TiAl composites, Synth. Sinter. 2 (2022) 138–145. https://doi.org/10.53063/synsint.2022.2383.
[8] H. Zhou, Z. Zhang, C. Liu, Q. Wang, Effect of Nd and Y on the microstructure and mechanical properties of ZK60 alloy, Mater. Sci. Eng: A. 445 (2007) 1–6. https://doi.org/10.1016/j.msea.2006.04.028.
[9] H. Li, H. Yang, Y. Zheng, F. Zhou, K. Qiu, X. Wang, Design and characterizations of novel biodegradable ternary Zn-based alloys with IIA nutrient alloying elements Mg, Ca and Sr, Mater. Des. 83 (2015) 95–102. https://doi.org/10.1016/j.matdes.2015.05.089.
[10] L.-C. Zhang, L.-Y. Chen, L. Wang, Surface modification of titanium and titanium alloys: technologies, developments, and future interests, Adv. Eng. Mater. 22 (2020) 1901258. https://doi.org/10.1002/adem.201901258.
[11] T. Chen, T. Shun, J. Yeh, M. Wong, Nanostructured nitride films of multi-element high-entropy alloys by reactive DC sputtering, Surf. Coat. Technol. 188 (2004) 193–200. https://doi.org/10.1016/j.surfcoat.2004.08.023.
[12] C.-Y. Hsu, J.-W. Yeh, S.-K. Chen, T.-T. Shun, Wear resistance and high-temperature compression strength of Fcc CuCoNiCrAl 0.5 Fe alloy with boron addition, Metall. Mater. Trans. A. 35 (2004) 1465–1469. https://doi.org/10.1007/s11661-004-0254-x.
[13] J.W. Yeh, S.K. Chen, S.J. Lin, J.Y. Gan, T.S. Chin, et al., Nanostructured high-entropy alloys with multiple principal elements: novel alloy design concepts and outcomes, Adv. Eng. Mater. 6 (2004) 299–303. https://doi.org/10.1002/adem.200300567.
[14] J.-W. Yeh, S.-J. Lin, T.-S. Chin, J.-Y. Gan, S.-K. Chen, et al., Formation of simple crystal structures in Cu-Co-Ni-Cr-Al-Fe-Ti-V alloys with multiprincipal metallic elements, Metall. Mater. Trans. A. 35 (2004) 2533–2536. https://doi.org/10.1007/s11661-006-0234-4.
[15] P.K. Huang, J.W. Yeh, T.T. Shun, S.K. Chen, Multi-principal-element alloys with improved oxidation and wear resistance for thermal spray coating, Adv. Eng. Mater. 6 (2004) 74–78. https://doi.org/10.1002/adem.200300507.
[16] B. Cantor, I. Chang, P. Knight, A. Vincent, Microstructural development in equiatomic multicomponent alloys, Mater. Sci. Eng: A. 375 (2004) 213–218. https://doi.org/10.1016/j.msea.2003.10.257.
[17] J. Qiao, E.-W. Huang, F. Jiang, T. Ungár, G. Csiszár, et al., Resolving ensembled microstructural information of bulk-metallic-glass-matrix composites using synchrotron X-ray diffraction, Appl. Phys. Lett. 97 (2010) 171910. https://doi.org/10.1063/1.3506694.
[18] K. Zhao, X. Xia, H. Bai, D. Zhao, W. Wang, Room temperature homogeneous flow in a bulk metallic glass with low glass transition temperature, Appl. Phys. Lett. 98 (2011) 141913. https://doi.org/10.1063/1.3575562.
[19] H. Lou, X. Wang, F. Xu, S. Ding, Q. Cao, et al., 73 mm-diameter bulk metallic glass rod by copper mould casting, Appl. Phys. Lett. 99 (2011) 051910. https://doi.org/10.1063/1.3621862.
[20] Y. Zhou, Y. Zhang, F. Wang, G. Chen, Phase transformation induced by lattice distortion in multiprincipal component CoCrFeNiCuxAl1−x solid-solution alloys, Appl. Phys. Lett. 92 (2008) 241917. https://doi.org/10.1063/1.2938690.
[21] X. Wang, Y. Zhang, Y. Qiao, G. Chen, Novel microstructure and properties of multicomponent CoCrCuFeNiTix alloys, Intermetallics. 15 (2007) 357–362. https://doi.org/10.1016/j.intermet.2006.08.005.
[22] Y. Zhou, Y. Zhang, Y. Wang, G. Chen, Solid solution alloys of AlCoCrFeNiTix with excellent room-temperature mechanical properties, Appl. Phys. Lett. 90 (2007) 181904. https://doi.org/10.1063/1.2734517.
[23] O. Senkov, G. Wilks, D. Miracle, C. Chuang, P. Liaw, Refractory high-entropy alloys, Intermetallics. 18 (2010) 1758–1765. https://doi.org/10.1016/j.intermet.2010.05.014.
[24] M.-H. Chuang, M.-H. Tsai, W.-R. Wang, S.-J. Lin, J.-W. Yeh, Microstructure and wear behavior of AlxCo1. 5CrFeNi1. 5Tiy high-entropy alloys, Acta Mater. 59 (2011) 6308–6317. https://doi.org/10.1016/j.actamat.2011.06.041.

[25] D. Miracle, B. Majumdar, K. Wertz, S. Gorsse, New strategies and tests to accelerate discovery and development of multi-principal element structural alloys, Scr. Mater. 127 (2017) 195–200. https://doi.org/10.1016/j.scriptamat.2016.08.001.
[26] D. Ma, B. Grabowski, F. Körmann, J. Neugebauer, D. Raabe, Ab initio thermodynamics of the CoCrFeMnNi high entropy alloy: Importance of entropy contributions beyond the configurational one, Acta Mater. 100 (2015) 90–97. https://doi.org/10.1016/j.actamat.2015.08.050.
[27] S. Varalakshmi, M. Kamaraj, B. Murty, Synthesis and characterization of nanocrystalline AlFeTiCrZnCu high entropy solid solution by mechanical alloying, J. Alloys Compd. 460 (2008) 253–257. https://doi.org/10.1016/j.jallcom.2007.05.104.
[28] Y. Jien-Wei, Recent progress in high entropy alloys, Ann. Chim. Sci. Mat. 31 (2006) 633–648. https://doi.org/10.3166/ACSM.31.633-648.
[29] G. Laplanche, A. Kostka, O. Horst, G. Eggeler, E. George, Microstructure evolution and critical stress for twinning in the CrMnFeCoNi high-entropy alloy, Acta Mater. 118 (2016) 152–163. https://doi.org/10.1016/j.actamat.2016.07.038.
[30] A.S. Sharma, S. Yadav, K. Biswas, B. Basu, High-entropy alloys and metallic nanocomposites: Processing challenges, microstructure development and property enhancement, Mater. Sci. Eng: R: Rep. 131 (2018) 1–42. https://doi.org/10.1016/j.mser.2018.04.003.
[31] S. Mamnooni, E. Borhani, H. Heydari, Is synthesizing a Cu35Co35Ni20Ti5Al5 high-entropy alloy beyond the rules of solid-solution formation?, Synth. Sinter. 3 (2023) 226–233. https://doi.org/10.53063/synsint.2023.34177.
[32] A.L. Greer, Confusion by design, Nature. 366 (1993) 303–304. https://doi.org/10.1038/366303a0.
[33] S. Mamnooni, E. Borhani, M. Shahedi Asl, Nanocrystalline Ni25Co20Cu10Fe25Mn20 High-Entropy Alloys Prepared by Mechanical Alloying, JOM. (2024) 1–12. https://doi.org/10.1007/s11837-024-06474-w.
[34] C.-J. Tong, Y.-L. Chen, J.-W. Yeh, S.-J. Lin, S.-K. Chen, et al., Microstructure characterization of Al x CoCrCuFeNi high-entropy alloy system with multiprincipal elements, Metall. Mater. Trans. A. 36 (2005) 881–893. https://doi.org/10.1007/s11661-005-0283-0.
[35] Y. Zhou, Y. Zhang, Y. Wang, G. Chen, Microstructure and compressive properties of multicomponent Alx (TiVCrMnFeCoNiCu) 100− x high-entropy alloys, Mater. Sci. Eng: A. 454 (2007) 260–265. https://doi.org/10.1016/j.msea.2006.11.049.
[36] R. Sonkusare, A. Swain, M. Rahul, S. Samal, N. Gurao, et al., Establishing processing-microstructure-property paradigm in complex concentrated equiatomic CoCuFeMnNi alloy, Mater. Sci. Eng: A. 759 (2019) 415–429. https://doi.org/10.1016/j.msea.2019.04.096.
[37] R. Wang, K. Zhang, C. Davies, X. Wu, Evolution of microstructure, mechanical and corrosion properties of AlCoCrFeNi high-entropy alloy prepared by direct laser fabrication, J. Alloys Compd. 694 (2017) 971–981. https://doi.org/10.1016/j.jallcom.2016.10.138.
[38] C.-J. Tong, M.-R. Chen, J.-W. Yeh, S.-J. Lin, S.-K. Chen, et al., Mechanical performance of the Al x CoCrCuFeNi high-entropy alloy system with multiprincipal elements, Metall. Mater. Trans. A. 36 (2005) 1263–1271. https://doi.org/10.1007/s11661-005-0218-9.
[39] Y. Chen, T. Duval, U. Hung, J. Yeh, H. Shih, Microstructure and electrochemical properties of high entropy alloys—a comparison with type-304 stainless steel, Corros. Sci. 47 (2005) 2257–2279. https://doi.org/10.1016/j.corsci.2004.11.008.
[40] G.D. Sathiaraj, P.P. Bhattacharjee, C.-W. Tsai, J.-W. Yeh, Effect of heavy cryo-rolling on the evolution of microstructure and texture during annealing of equiatomic CoCrFeMnNi high entropy alloy, Intermetallics. 69 (2016) 1–9. https://doi.org/10.1016/j.intermet.2015.10.005.
[41] Z. Li, S. Zhao, R.O. Ritchie, M.A. Meyers, Mechanical properties of high-entropy alloys with emphasis on face-centered cubic alloys, Prog. Mater. Sci. 102 (2019) 296–345. https://doi.org/10.1016/j.pmatsci.2018.12.003.
[42] S. Sinha, S. Nene, M. Frank, K. Liu, R. Mishra, et al., Microstructural evolution and deformation behavior of Ni-Si-and Co-Si-containing metastable high entropy alloys, Metall. Mater. Trans. A. 50 (2019) 179–190. https://doi.org/10.1007/s11661-018-4968-6.
[43] Z. Lyu, X. Fan, C. Lee, S.-Y. Wang, R. Feng, P.K. Liaw, Fundamental understanding of mechanical behavior of high-entropy alloys at low temperatures: A review, J. Mater. Res. 33 (2018) 2998–3010. https://doi.org/10.1557/jmr.2018.273.
[44] Z. Wu, M.C. Troparevsky, Y. Gao, J.R. Morris, G.M. Stocks, H. Bei, Phase stability, physical properties and strengthening mechanisms of concentrated solid solution alloys, Curr. Opin. Solid State Mater. Sci. 21 (2017) 267–284. https://doi.org/10.1016/j.cossms.2017.07.001.
[45] Y. Zhang, T.T. Zuo, Z. Tang, M.C. Gao, K.A. Dahmen, et al., Microstructures and properties of high-entropy alloys, Prog. Mater. Sci. 61 (2014) 1–93. https://doi.org/10.1016/j.pmatsci.2013.10.001.
[46] M.-H. Tsai, J.-W. Yeh, High-entropy alloys: a critical review, Mater. Res. Lett. 2 (2014) 107–123. https://doi.org/10.1080/21663831.2014.912690.
[47] T.-T. Shun, L.-Y. Chang, M.-H. Shiu, Microstructure and mechanical properties of multiprincipal component CoCrFeNiMox alloys, Mater. Charact. 70 (2012) 63–67. https://doi.org/10.1016/j.matchar.2012.05.005.
[48] T.-T. Shun, L.-Y. Chang, M.-H. Shiu, Microstructures and mechanical properties of multiprincipal component CoCrFeNiTix alloys, Mater. Sci. Eng: A. 556 (2012) 170–174. https://doi.org/10.1016/j.msea.2012.06.075.
[49] D.B. Miracle, O.N. Senkov, A critical review of high entropy alloys and related concepts, Acta Mater. 122 (2017) 448–511. https://doi.org/10.1016/j.actamat.2016.08.081.
[50] H. Heydari, M. Tajally, A. Habibolahzadeh, Computational analysis of novel AlLiMgTiX light high entropy alloys, Mater. Chem. Phys. 280 (2022) 125834. https://doi.org/10.1016/j.matchemphys.2022.125834.
[51] S. Guo, C. Ng, J. Lu, C. Liu, Effect of valence electron concentration on stability of fcc or bcc phase in high entropy alloys, J. Appl. Phys. 109 (2011) 103505. https://doi.org/10.1063/1.3587228.
[52] G. Sheng, C.T. Liu, Phase stability in high entropy alloys: Formation of solid-solution phase or amorphous phase, Prog. Nat. Sci: Mater. Int. 21 (2011) 433–446. https://doi.org/10.1016/S1002-0071(12)60080-X.
[53] V. Shivam, J. Basu, Y. Shadangi, M.K. Singh, N. Mukhopadhyay, Mechano-chemical synthesis, thermal stability and phase evolution in AlCoCrFeNiMn high entropy alloy, J. Alloys Compd. 757 (2018) 87–97. https://doi.org/10.1016/j.jallcom.2018.05.057.
[54] Y. Dong, Y. Lu, L. Jiang, T. Wang, T. Li, Effects of electro-negativity on the stability of topologically close-packed phase in high entropy alloys, Intermetallics. 52 (2014) 105–109. https://doi.org/10.1016/j.intermet.2014.04.001.
[55] S. Mamnooni, E. Borhani, M.S. Asl, Feasibility of using Ni25Co20Cu10Fe25Mn20 high entropy alloy as a novel sintering aid in ZrB2 ceramics, Ceram. Int. (2024). https://doi.org/10.1016/j.ceramint.2024.03.102.